Oceanic calcium changes from enhanced weathering during the Paleocene-Eocene thermal maximum: No effect on calcium-based proxies

N. Komar[1] and R. E. Zeebe[1]

[1] During the Paleocene-Eocene thermal maximum (PETM ~55 Myr ago), prominent climatic and biogeochemical changes took place in the atmosphere, ocean, and on land. For example, deep-sea temperatures rose by 5°C to 6°C, while sea surface temperatures at high latitudes increased by up to 9°C. In the sedimentary record, the onset of the PETM is marked by widespread dissolution of calcium carbonate on the seafloor. In addition, there is evidence for globally higher humidity, precipitation and increased weathering during the PETM. Both calcium carbonate dissolution and enhanced weathering probably affected the seawater calcium concentration. Here we investigate implications that possible changes in the ocean's calcium inventory may have had on boron/calcium (B/Ca) and magnesium/calcium (Mg/Ca) ratios, which are used as proxies for deep water carbonate chemistry and temperature, respectively. We also examine effects on δ^{44}Ca of seawater, which is used as an indicator for variations in the marine calcium cycle. We focus on the magnitude of change in the ocean's calcium ion concentration as a result of the carbon perturbation, which resulted in increased weathering fluxes and the dissolution of calcite on the ocean floor during the PETM. Different ranges of carbon input scenarios and their effect on ocean chemistry were examined using the Long-term Ocean-atmosphere-Sediment CArbon cycle Reservoir (LOSCAR) model. We found that under the most plausible scenario, the calcium ion concentration change ($\Delta[Ca^{2+}]$) was less than 0.7% and around 2% in the most extreme scenario. Our results show that B/Ca and Mg/Ca proxies were not affected within analytical precision by changes in oceanic calcium due to weathering and carbonate dissolution during the PETM. The most extreme scenario ($\Delta[Ca^{2+}] = 2\%$) would result in ~4 μmol kg^{-1} uncertainty in reconstruction of $\Delta[CO_3^{2-}]$. The same scenario affects the temperature reconstruction by ~0.2°C. The effect on the ocean's calcium isotope budget was insignificant as well, resulting in $\Delta\delta^{44}Ca_{sw}$ of less than 0.05‰.
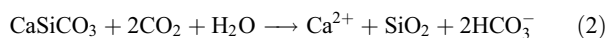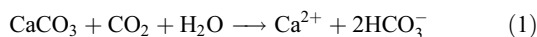
1. Introduction

[2] The Paleocene-Eocene thermal maximum (PETM) took place around 55 million years ago. During the event, sea surface temperatures increased by 5–9°C in low and high latitudes [e.g., *Zachos et al.*, 2003; *Sluijs et al.*, 2006]. *Kennett and Stott* [1991] observed a 2.5‰ decline in the δ^{13}C of calcium carbonate in foraminifera from the Southern Ocean. This decrease was most likely due to the introduction of isotopically light carbon into the ocean-atmosphere system [e.g., *Koch et al.*, 1992; *Dickens et al.*, 1995; *Zachos 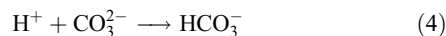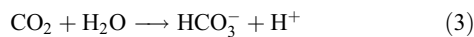et al.*, 2001; *Dunkley Jones et al.*, 2010]. By using a simple mass balance equation it is possible to estimate the mass of carbon needed for a −2.5‰ carbon isotope excursion, given the isotopic composition of the source. In the past, three different sources have usually been considered: carbon from the mantle (δ^{13}C = −5‰), carbon in organic matter (δ^{13}C = −25‰), and carbon as methane (δ^{13}C= −60‰). Conversely, if the carbon input mass was known, it would be possible to constrain the sources because of their different carbon isotope compositions. The different sources have led to speculations concerning the mechanism. Some, such as volcanic intrusion, imply that the carbon drives the warming. Others, such as destabilization of oceanic methane hydrates imply that the carbon release is a feedback that can exacerbate warming [*Dickens et al.*, 1995; *Dickens*, 2000; *Pagani et al.*, 2006]. Modeling of the carbon cycle during the PETM indicates that the initial carbon pulse was around 3,000 Pg C [*Zeebe et al.*, 2009]. The intrusion of such a large amount of

[1]Department of Oceanography, School of Ocean and Earth Science and Technology, University of Hawaii at Manoa, Honolulu, Hawaii, USA.

carbon into the ocean-atmosphere system had a series of consequences that affected the chemistry and biology of the oceans [e.g., *Zachos et al.*, 2005; *Thomas*, 2007; *Webb et al.*, 2009]. There are several lines of evidence indicating intensified weathering rates during the PETM. For instance, the osmium isotopic composition of seawater became more radiogenic during this period, indicating an accelerated hydrologic cycle and consequently enhanced weathering [*Ravizza et al.*, 2001]. Furthermore, increased kaolinite abundances during the recovery stages of the PETM also indicate increased runoff rates [*Kelly et al.*, 2005; *Ravizza et al.*, 2001; *Robert and Kennett*, 1994]. The increase in both temperature and pCO_2 most likely led to enhanced silicate and carbonate weathering fluxes, which increased the calcium input to the ocean:

$$CaCO_3 + CO_2 + H_2O \longrightarrow Ca^{2+} + 2HCO_3^- \qquad (1)$$

$$CaSiCO_3 + 2CO_2 + H_2O \longrightarrow Ca^{2+} + SiO_2 + 2HCO_3^- \qquad (2)$$

[3] Another consequence of the large carbon input into the ocean-atmosphere system was extensive calcite dissolution that took place on the ocean's floor. The dissolution was due to the depletion of carbonate ion in seawater:

$$CO_2 + H_2O \longrightarrow HCO_3^- + H^+ \qquad (3)$$

$$H^+ + CO_3^{2-} \longrightarrow HCO_3^- \qquad (4)$$

In general, the rate of deposition/dissolution of calcite to/from sediments depends on the saturation state of seawater. The stability is related to the concentrations of Ca^{2+} and CO_3^{2-} via the saturation state of the solution ($\Omega = [Ca^{2+}] \times [CO_3^{2-}]/K_{sp}^*$), where K_{sp}^* is the solubility product of the calcium carbonate mineral in question (e.g., calcite or aragonite). Thus, deposition/dissolution depends on $[Ca^{2+}]$ and $[CO_3^{2-}]$ in seawater and K_{sp}^*, which increases with depth. The equilibrium calcite saturation horizon is the depth at which $\Omega = 1$. Below this point dissolution proceeds and $\Omega < 1$. With increasing depth, Ω decreases and the rate of dissolution increases. The depth at which dissolution is balanced by the rain of calcite to the sediments is known as the calcite compensation depth (CCD) [e.g., *Ridgwell and Zeebe*, 2005].

[4] The intrusion of CO_2 into the seawater during the PETM resulted in rapid shoaling of the CCD (in less than 10 ky) by more than 2 km in the Atlantic Ocean [*Zachos et al.*, 2005]. The decrease in $[CO_3^{2-}]$ resulted in increased area of undersaturation producing a shallower CCD, instigating the dissolution of calcite and thus additional input of calcium to the ocean. The decline in CO_3^{2-} (in combination with O_2 depletion) affects the stability and production of $CaCO_3$ minerals, which may have affected benthic foraminifera during the PETM, causing major extinctions [*Kennett and Stott*, 1991; *Thomas*, 2007; *Ridgwell and Schmidt*, 2010].
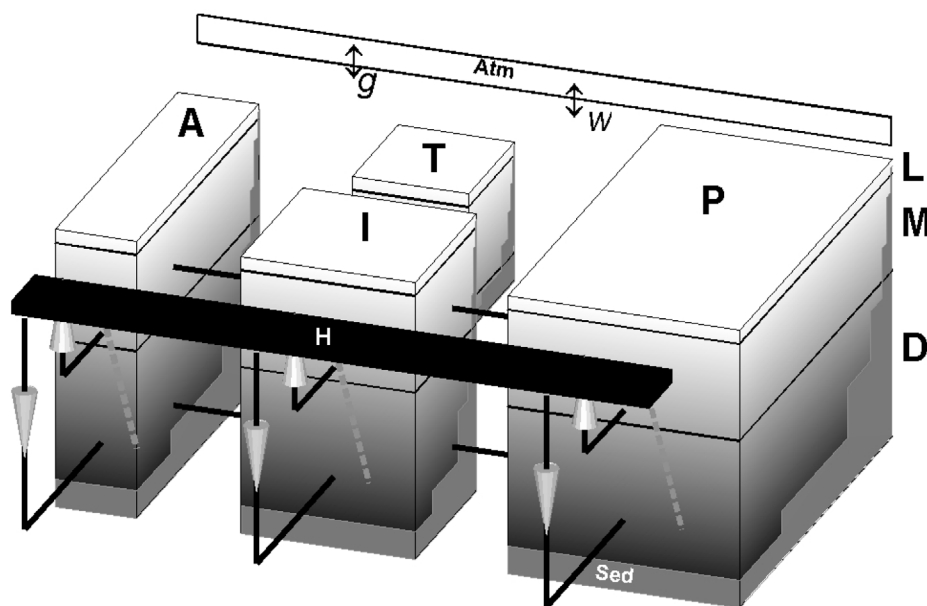
[5] The increased weathering as well as dissolution of calcite from the seafloor might have caused significant changes in the ocean's calcium inventory during the PETM. In this study, we assess potential artifacts induced in Ca-based proxies due to a changing ocean calcium inventory. There are several methods which use Ca-based proxies as a tool for deciphering paleoenvironmental changes. Past changes in the concentration of CO_3^{2-} are not easy to quantify even though many studies have been carried out to investigate it. The difficulties are mostly due to the limitations of the different methods (proxies based on carbonate dissolution, theory and empirical relationships) [e.g., *Yu and Elderfield*, 2007]. Nonetheless, *Yu et al.* [2007] have developed a new method to reconstruct deep water chemistry, which is based on boron/calcium (B/Ca) ratios in benthic foraminifera. They found a correlation between benthic foraminiferal B/Ca and $\Delta[CO_3^{2-}]$ (the degree of carbonate saturation), which provides a paleoproxy for deep water $[CO_3^{2-}]$. Furthermore, *Elderfield and Ganssen* [2000] and many others [e.g., *Rosenthal et al.*, 1997; *Lea et al.*, 2000; *Dekens et al.*, 2002; *Zachos et al.*, 2003] have applied another correlation in planktonic and benthic foraminifera, which also involves the calcium concentration. The magnesium/calcium (Mg/Ca) ratio in foraminifera shows a temperature dependence and is thus being used widely as a proxy for determining past records of temperature. In this study, we also examine the effect of the marine calcium concentration and increased weathering on the Ca isotope composition of seawater ($\delta^{44}Ca_{sw}$), which is used as an indicator for variations in the marine calcium cycle [e.g., *Fantle and DePaolo*, 2005; *Heuser et al.*, 2005; *Griffith et al.*, 2008; *Fantle*, 2010].

[6] In the studies mentioned above, it is assumed that $[Ca^{2+}]$ in seawater remained constant over relatively short time-scales because of the long residence time of calcium in the ocean (1 to 2 Ma). In this study, we modeled the changes in the deep ocean chemistry during the PETM, primarily focusing on possible changes in the inventory of Ca^{2+} which, if large enough, could have affected the validity of the above mentioned proxies. In order to determine whether enhanced weathering and deep sea dissolution can significantly alter the Ca^{2+} inventory of the sea, we conducted simulations using a long-term carbon cycle model [*Zeebe et al.*, 2008; *Zachos et al.*, 2008; *Zeebe et al.*, 2009]. We consider different scenarios by exposing the system to a wide range of carbon inputs (1,000 Pg C to 6,000 Pg C) and weathering parameterizations, i.e., we effectively vary the magnitude of carbonate dissolution and weathering fluxes (see below).

2. Dissolution: Back-of-the-Envelope Calculation

[7] As previously mentioned, there are at least two mechanisms (terrestrial weathering and dissolution from the seafloor) that could have altered the ocean's $[Ca^{2+}]$ during the PETM. Estimating the effect on $[Ca^{2+}]$ that is caused solely by dissolution is relatively easy and is explained in this section and Appendix A. If the initial position of the CCD was at 3.5 km and if we assume that the entire ocean floor above that depth (shallower than 3.5 km) underwent dissolution, we calculate that $[Ca^{2+}]$ would have changed by approximately 0.4% (assuming that porosity varies with % $CaCO_3$; see Appendix A). Thus, an estimate of the dissolution effect on the ocean's calcium budget can be obtained without the use of numerical models. However, the effects of weathering on $[Ca^{2+}]$ are more complex and not easily predictable *a priori*. It turned out that the transient changes in seawater $[Ca^{2+}]$ are controlled by a time-dependent balance between river input and sediment burial, where the

Figure 1. Schematic view of the LOSCAR model. The arrows indicate SO deep water formation; A, I, P, and T stand for the Atlantic, Indian, Pacific, and Tethys ocean; H is a high latitude box; L, M, and D correspond to low, intermediate, and deep ocean boxes; "g" is gas exchange, and "w" is weathering.

magnitude of change differs in response to carbonate and silicate weathering (see Discussion). Such features are difficult to quantify based on a back-of-the-envelope calculation. Here we employ a numerical modeling approach to addressed both, effects of dissolution and weathering on the seawater calcium concentration during the PETM.

3. Model Description

[8] The model used in this study is the LOSCAR (Long-term Ocean-atmosphere-Sediment CArbon cycle Reservoir) model (Figure 1). It is a modified version of the carbon cycle model developed by *Walker and Kasting* [1992], coupled to a sediment module [*Zeebe and Zachos*, 2007]. It represents the ocean basin bathymetry of earlier geologic times, such as the Paleocene-Eocene era. In addition to the Atlantic (A), Indic (I) and Pacific (P) basin, the Tethys (T) ocean is also included. Each of these four ocean basins are subdivided into three boxes, which correspond to the low-latitude surface ocean (L), the intermediate water masses (M) and the deep ocean (D). There is also an additional box that represents the high latitude ocean (H). The model uses realistic volumes of ocean basins based on Paleocene-Eocene topography [*Bice and Marotzke*, 2002]. Prior to the PETM, deepwater formation in the model was prescribed to occur in the Southern Ocean (SO), consistent with observations [*Thomas et al.*, 2003]. After the PETM main phase, a steady contribution of North Pacific Deep Water formation was assumed (the SO source remains active but is reduced relative to its pre-event strength). After ~70 ky, the NP source is shut off and SO formation returns to pre-event levels. The model includes biogeochemical cycles of total carbon, total alkalinity, phosphate, oxygen, stable carbon isotopes, and calcium.

[9] Ocean carbonate chemistry routines to calculate parameters such as $[CO_2]$, $[CO_3^{2-}]$, pH, and calcite saturation state from total CO_2 and total alkalinity use algorithms as described by *Zeebe and Wolf-Gladrow* [2001]. Routines that allow for variations in the Ca^{2+} and Mg^{2+} concentration of seawater, which most likely differed from modern values during the Paleocene-Eocene are described by *Tyrrell and Zeebe* [2004]. In our PETM simulations we used $[Ca^{2+}]$ = 20 mmol kg^{-1} and $[Mg^{2+}]$ = 30 mmol kg^{-1} as inferred from fluid inclusions in marine halites [*Lowenstein et al.*, 2001; *Horita et al.*, 2002], rather than the modern values of $[Ca^{2+}]$ = 10 mmol kg^{-1} and $[Mg^{2+}]$ = 53 mmol kg^{-1} [*Tyrrell and Zeebe*, 2004]. (Note that our conclusions also hold at modern seawater Ca and Mg concentrations, as additional simulations showed). Warmer surface and bottom water temperatures in the late Paleocene and Eocene also impact equilibrium and solubility constants. For example, the calcite saturation concentration at a bottom water temperature of 14–17°C during the PETM is quite different from the modern temperature of ~2°C. In the model, we used bottom water temperatures of 12°C and 16°C prior to and during the PETM, respectively, and included the effects of changes in temperature, and $[Ca^{2+}]$ and $[Mg^{2+}]$ on the stoichiometric equilibrium constants.

[10] The model runs were performed under a suite of carbon emission scenarios, with an initial pulse ranging from 1,000 to 6,000 Pg C (covering the range of scenarios discussed in the literature [*Dickens et al.*, 1995; *Panchuk et al.*, 2008]) and a release time over 6 ky [*Zeebe et al.*, 2009]. The model was run for 200 ky in total, the time span during which calcium changes are important (the onset of calcium change is within this time range as well as the essential stage of the carbonate ion recovery phase). Additionally, effects of silicate weathering are observed on this timescale. Observations indicate that atmospheric CO_2, temperature and precipitation increased during the PETM as a result of the carbon perturbation, which enhances terrestrial weathering of carbonate and silicate rocks [*Berner et al.*, 1983; *White and Blum*, 1995;

Ravizza et al., 2001; *Schmitz and Pujalte*, 2007]. In the model, the carbonate (F_C) and silicate (F_{Si}) weathering fluxes are parameterized as a function of atmospheric CO_2. In the model, this is expressed as:

$$F_{Si} = F_{Si}^0 \times \left(pCO_2/pCO_2^0\right)^{n_{Si}} \qquad (5)$$

$$F_C = F_C^0 \times \left(pCO_2/pCO_2^0\right)^{n_{CC}} \qquad (6)$$

where (F_C^0) and (F_{Si}^0) are initial carbonate and silicate weathering fluxes for the PETM, set at 15.8×10^{12} mol C yr^{-1} and 5.7×10^{12} mol C yr^{-1}, respectively (volcanic input equals silicate weathering flux). The modern weathering carbonate flux is $\sim12 \times 10^{12}$ [*Morse and Mackenzie*, 1990] and silicate and mantle/volcanic CO_2 outgassing fluxes are $\sim5 \times 10^{12}$ mol C yr^{-1} [*Walker and Kasting*, 1992].

[11] The rationale for having the pre-PETM fluxes initially set higher than the modern values was to account for accelerated weathering influx during the Paleocene due to higher pCO_2 and higher temperature. Carbonate rain to the seafloor within the model is split into two broad locations: shelf/upper slope (<600 m) and lower slope/rise/plains (>600 m). The pre-PETM ratio of shallow-to-deep carbonate rain was increased relative to the modern because sea level was higher, which promotes shallow water marine carbonate deposition (as has been documented for the Paleocene and Early Eocene [e.g., *Kiessling et al.*, 2003]). In general, observations imply relatively less pelagic carbonate production during the early Cenozoic, which leads to a shallower CCD compared to the modern in agreement with the observations [*Tyrrell and Zeebe*, 2004]. *Ravizza et al.* [2001] estimate increased PETM weathering by 23%–26%, if the Os isotope excursion was solely due to higher continental flux. The initial baseline atmospheric CO_2 concentration is represented by pCO_2^0 in the model and was set at 1,000 ppm. During the course of the simulation, atmospheric pCO_2 is predicted by the model and as it varies, it affects the rate of weathering of carbonate and silicate rocks. By default, silicate and carbonate weathering parameters (n_{Si} and n_{CC}) were set at 0.2 and 0.4, respectively. These values are at the lower end of the spectrum commonly used in the literature (conservative estimates) [*Walker et al.*, 1981; *Berner and Kothavala*, 2001; *Zeebe et al.*, 2008; *Zachos et al.*, 2008; *Uchikawa and Zeebe*, 2008; *Zeebe et al.*, 2009].

[12] We investigated the effects of increased weathering on the [Ca^{2+}] inventory with three different sets of parameter values. Scenario 1: enhanced carbonate weathering (n_{CC} varied between 0.4 and 1.4, n_{Si} kept constant at 0.2), Scenario 2: enhanced silicate weathering (n_{CC} kept constant at 0.4, n_{Si} varied between 0.2 and 1.2), and Scenario 3: enhanced carbonate as well as silicate weathering (n_{CC} and n_{Si} simultaneously varied between 0.4 and 1.4 and 0.2 and 1.2, respectively). The weathering parameterization used in this study is based on *Uchikawa and Zeebe* [2008].
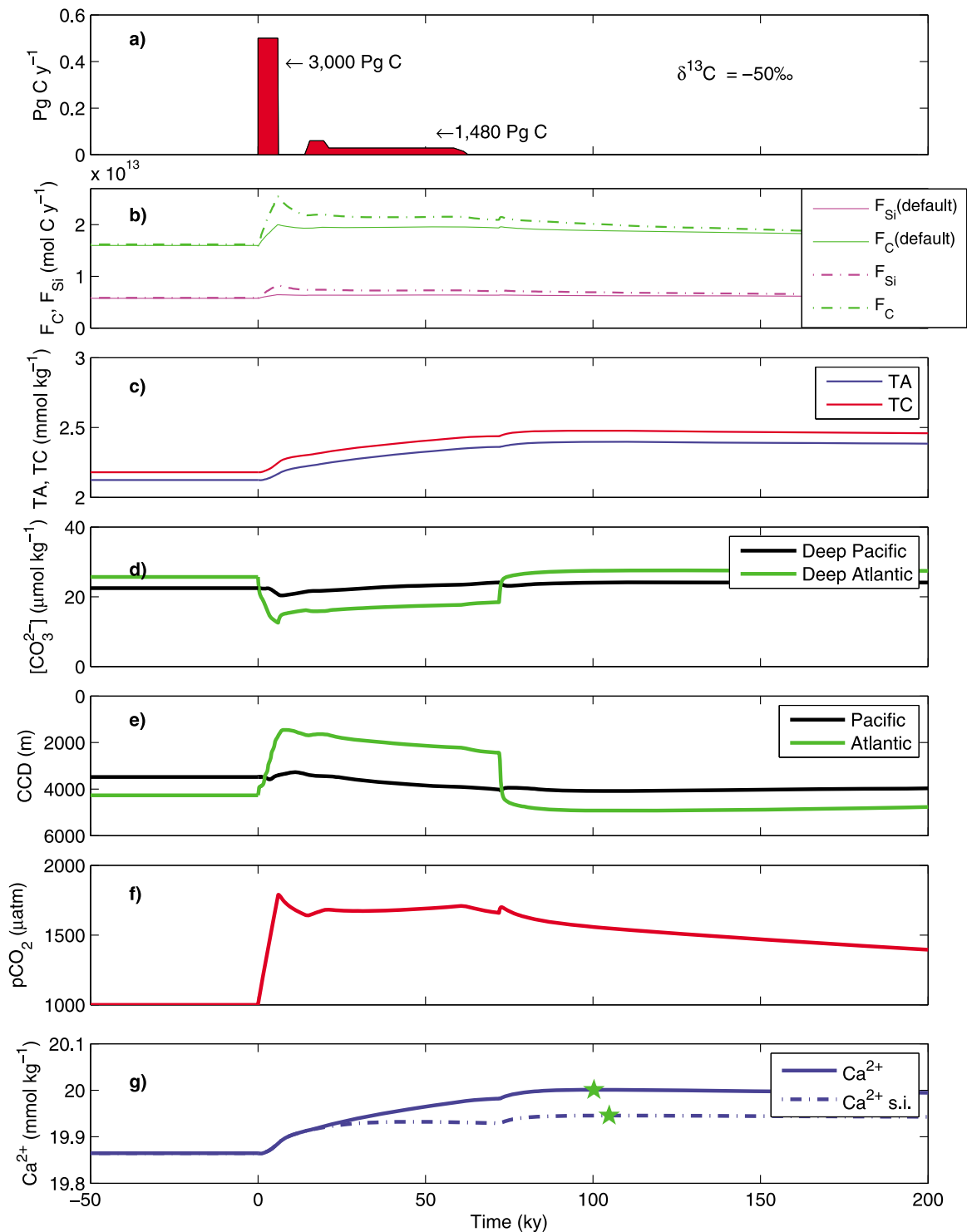
4. Results

[13] The results presented in Figure 2 correspond to the PETM model simulation in which carbonate and silicate weathering parameters were kept constant at default values (n_{CC} = 0.4, n_{Si} = 0.2) and the total carbon input was 3,000 Pg

over the first 6 ky, which is the most likely scenario according to *Zeebe et al.* [2009]. Figure 2a shows our PETM carbon release scenario, where t = 0 corresponds to the onset of the PETM (Paleocene-Eocene boundary). It is important to note that besides this large initial pulse, an additional smaller pulse was simulated, followed by a continuous carbon release (~1,500 Pg C). This prolonged carbon release is necessary to simulate the observed duration of deep-sea carbonate dissolution [see *Zeebe et al.*, 2009]. Without the additional release, the model was unable to reproduce the carbon isotope excursion duration because $\delta^{13}C$ values returned to pre-excursion values too quickly [*Zeebe et al.*, 2009]. Furthermore, the results of this simulation (a pulsed carbon release rather than a single input peak) are more consistent with $\delta^{13}C$ records [*Dickens*, 2001; *Bowen et al.*, 2004]. The prolonged carbon release is also important to simulate the observed duration of deep-sea carbonate dissolution [*Zeebe et al.*, 2009]. The extended duration of the dissolution event could not be reproduced in the model without the continued carbon release.
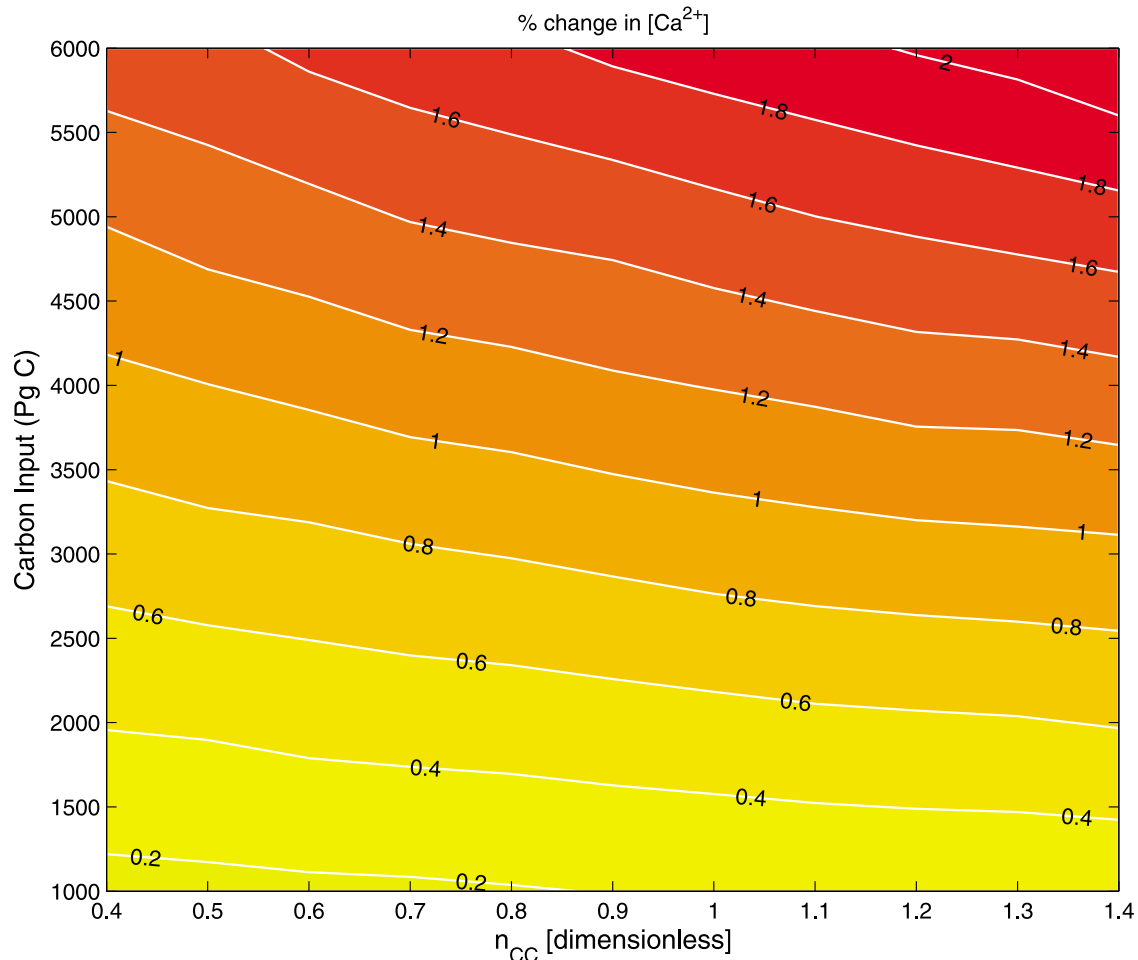
[14] A pulsed carbon release versus a single input peak results in a slightly larger maximum Ca^{2+} change in our study, 0.69% versus 0.41% respectively (Figure 2g; dotted line represents single input scenario). Thus, most of the dissolution takes place during the initial phase and any subsequent smaller input of carbon has an additional effect on maximum seawater [Ca^{2+}] change. For the case shown here in which carbonate and silicate weathering feedbacks are weak, this subsequent, additional carbon input prolongs the interval of Ca^{2+} perturbation and causes a time lag between the [Ca^{2+}] peak (around 100 ky) and the initial carbon input peak. Increase in both carbonate and silicate weathering rates are shown in Figure 2b (moles yr^{-1}). Solid lines (default n_{CC} and n_{Si}) and dashed lines (n_{CC} and n_{Si} are 0.9 and 0.7, respectively) compare the effect of carbonate and silicate weathering parameters on the magnitude of weathering. Figure 2c displays changes in total alkalinity (TA) and total carbon (TC). Simulated atmospheric pCO_2 is shown in Figure 2f. All of the above mentioned parameters (TA, TC, [CO_3^{2-}], CCD, [Ca^{2+}]), which are summarized in Figure 2, pertain to the deep Pacific ocean. The deep Pacific ocean was arbitrarily chosen because it represents the largest basin. Moreover, the differences in [Ca^{2+}] between the basins are negligible.

[15] The maximum deep ocean [Ca^{2+}] change (in percent) under the three different conditions of increased weathering (as described in section 1), as well as carbon input, are shown in Figures 3–5. Enhanced carbonate weathering (Figure 3), enhanced silicate weathering (Figure 4) and simultaneous increase of both carbonate and silicate weathering (Figure 5), correspond to scenarios 1, 2 and 3, respectively.

[16] Under the weathering scenario 1 (n_{CC} varied between 0.4 and 1.4, n_{Si} kept constant at 0.2), the simulated maximum deep ocean Ca^{2+} concentration increase (Δ[Ca^{2+}]) ranges from 0.14% to 2.07% (Figure 3). Δ[Ca^{2+}] is the ratio of maximum [Ca^{2+}] over the initial [Ca^{2+}] expressed in percent. The magnitude of Δ[Ca^{2+}] is most sensitive to the amount of carbon released (ranges from 1,000 to 6,000 Pg), whereas the increased sensitivity of carbonate weathering has a minor effect on Δ[Ca^{2+}]. Even when the carbonate weathering parameter n_{CC} is raised to 1.4 the change in

Figure 2. (a) PETM carbon release scenario. Here t = 0 corresponds to the onset of the PETM (Paleocene-Eocene boundary). (b) Increase in both carbonate (green) and silicate weathering (magenta) rates. Solid lines represent default weathering feedback (n_{CC} = 0.4 and n_{Si} = 0.2). Dashed lines represent increased weathering feedback n_{CC} = 0.9 and n_{Si} = 0.7. This shows that the increased feedback results in higher weathering rates. (c) TA (blue) and TC (red) of the Deep Pacific. (d) $[CO_3^{2-}]$ of the Deep Pacific (black) and the Deep Atlantic (green). (e) Simulated CCD changes in the Pacific (black) and Atlantic (green) oceans. (f) Simulated atmospheric pCO$_2$. (g) $[Ca^{2+}]$ of the Deep Pacific. The solid line represents the change in Ca^{2+} as a result of initial plus continuous input shown in Figure 2a, whereas the dashed line represents the change in Ca^{2+} as result of a single input (s.i.). The green stars represent the points of max Ca^{2+} concentration.

Figure 3. Simulated change in $[Ca^{2+}]$ as a function of carbon input and increased carbonate weathering flux. The silicate weathering flux was kept constant at the initial value of 5.7×10^{12} mol C yr^{-1}, $n_{Si} = 0.2$.
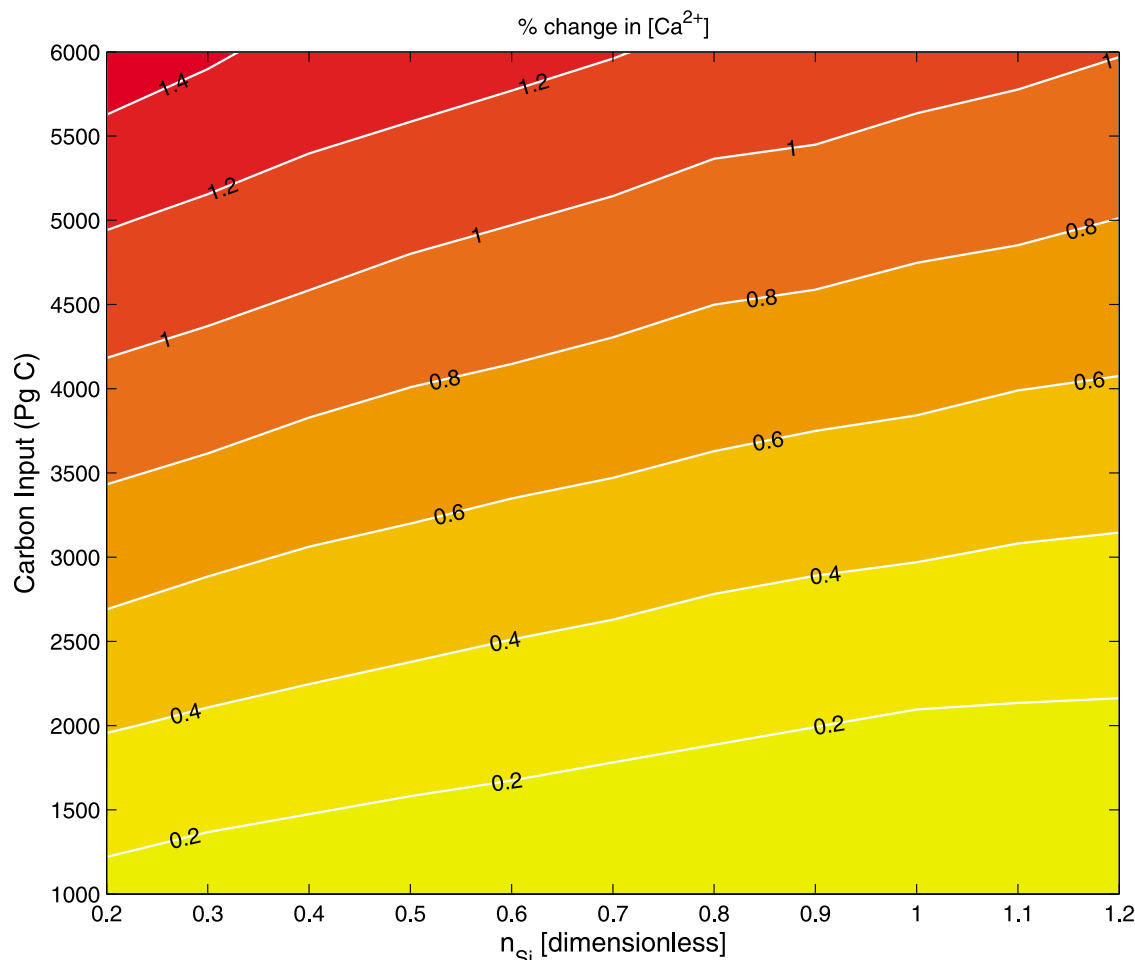
$[Ca^{2+}]$ is insignificant (for constant carbon input). Similar to scenario 1, the weathering scenario 2 (n_{CC} kept constant at 0.4, n_{Si} varied between 0.2 and 1.2) also shows that $\Delta[Ca^{2+}]$ strongly depends on the amount of carbon input. Under this scenario, the increased silicate weathering also has a minor effect on $\Delta[Ca^{2+}]$. However, under this scenario, the $\Delta[Ca^{2+}]$ decreases as the silicate weathering flux increases (Figure 4). The reason for this is that the increased silicate flux increases the total alkalinity (but it does not increase total carbon, unlike carbonate weathering) of the deep ocean, allowing the CCD to deepen. This results in a larger area of the ocean supersaturated with respect to calcite preserving calcium carbonate falling from the surface (carbonate burial), which consequently decreases the amount of dissolved Ca^{2+} (see discussion for more information).

[17] Silicate and carbonate weathering both depend on atmospheric CO_2, thus it is unlikely that they increased independently from each other during the PETM. Therefore another set of simulations, which assumes concurrent increase in the sensitivity of carbonate and silicate weathering was conducted (weathering scenario 3). Under this scenario, carbonate and silicate weathering sensitivity parameters were simultaneously varied over a range of values covering the most plausible scenarios (n_{CC} was increased from 0.4 to 1.4 and n_{Si} was simultaneously increased between 0.2 and 1.2).

Figure 5 shows the magnitude of $\Delta[Ca^{2+}]$ as a function of carbon input (1,000 to 6,000 Pg) and enhanced carbonate and silicate weathering rates (which result from increased n_{CC} and n_{Si} as follows from equations (5) and (6); see Figure 2b). As seen in the two other scenarios, the $\Delta[Ca^{2+}]$ essentially only depends on the amount of carbon input, with almost no visible effect from enhanced weathering. The $\Delta[Ca^{2+}]$ ranges from 0.07 to 1.51%.
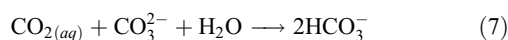
5. Discussion

[18] The model used in our study shows that dissolution as well as enhanced carbonate and silicate weathering rates have a small effect on the ocean's calcium inventory during the PETM, even though the rate of delivery of Ca^{2+} from the land to the ocean probably increased significantly. The reason for this is that after ~10 ky enhanced weathering increases the calcite saturation state of the deep ocean. As a consequence, the CCD deepens, leading to an increased burial of calcite because a larger area of the seafloor is bathed in supersaturated water [*Zeebe and Westbroek*, 2003]. Therefore, the process of increased weathering (adding Ca^{2+}) is almost compensated for by the process of increased burial (removing Ca^{2+}) even though the compensation is not instantaneous (there is a time lag between

Figure 4. Simulated change in $[Ca^{2+}]$ as a function of carbon input and increased silicate weathering flux. The carbonate flux was kept constant at the initial value of 15.8×10^{12} mol C yr^{-1}, $n_{CC} = 0.4$.

the response in the CCD to increased weathering rates). This time lag enables $[Ca^{2+}]$ to increase but this increase has an insignificant effect on the CCD change. Thus weathering has a minor effect on the change of calcium inventory over millennial timescales (Figure 5).

[19] On the other hand, the $\Delta[Ca^{2+}]$ strongly depends on the carbon input (Figure 5). As it was earlier explained and shown in Figure 3, CO_2 reacts in seawater to produce mostly HCO_3^-. The input of CO_2 (3,000 Pg C over the first 6 ky in our model run) to the ocean increases the dissolved inorganic carbon in seawater (Figure 2c). As a result, the $[CO_3^{2-}]$ declines (Figure 2d), lowering the saturation state of seawater with respect to carbonate minerals [*Zeebe and Wolf-Gladrow*, 2001; *Ridgwell and Zeebe*, 2005]. This decrease in $[CO_3^{2-}]$ can be illustrated by combining equations (3) and (4) to get the following aqueous carbonate equilibrium reaction:
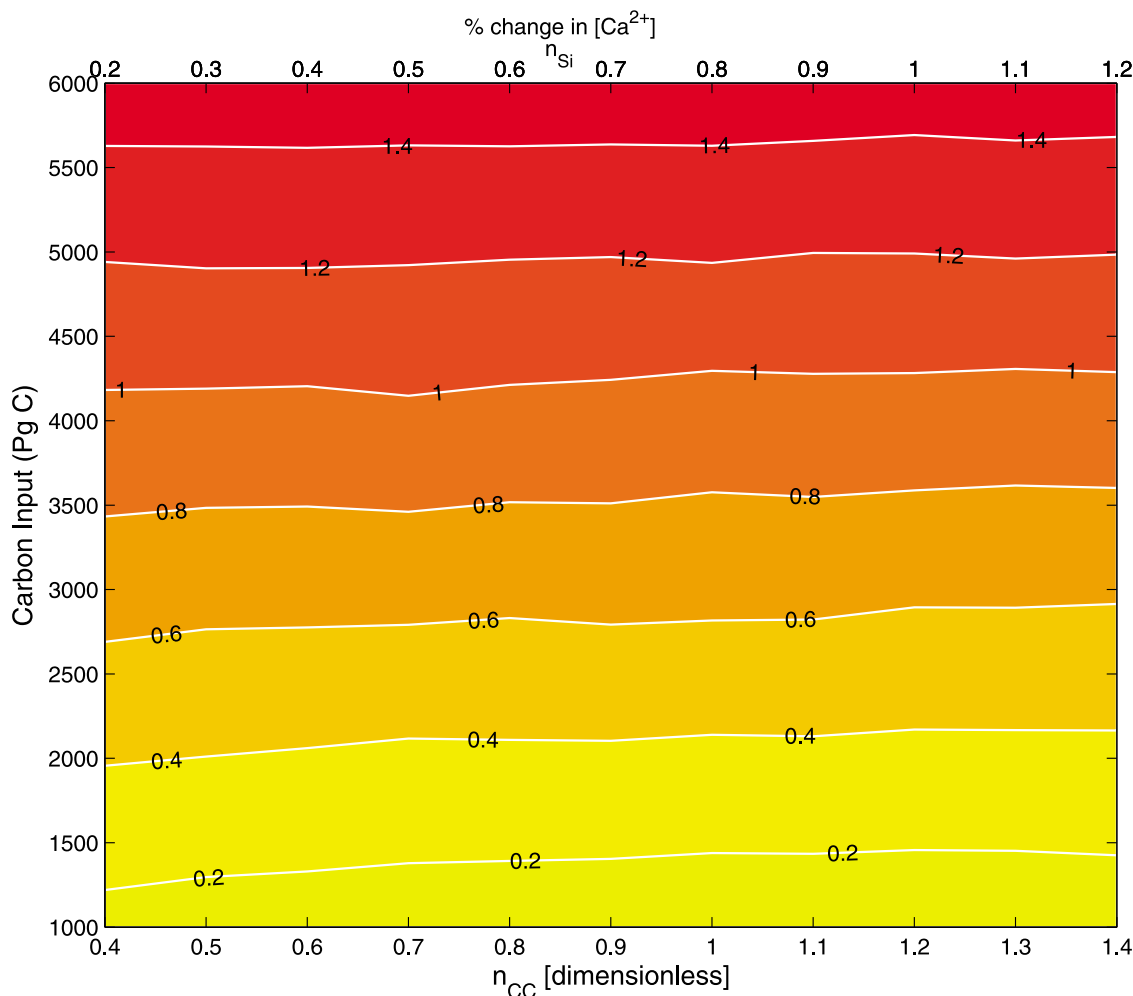
$$CO_{2(aq)} + CO_3^{2-} + H_2O \longrightarrow 2HCO_3^- \qquad (7)$$

With increased $CO_{2(aq)}$, there is a removal of CO_3^{2-} and an increase of bicarbonate. With a decrease of CO_3^{2-}, the CCD shoals. The global CCD (average CCD of all ocean basins) shoals by approximately 0.75 km as a result of the carbon input (simulation shown in Figure 2), whereas the CCD in the

Pacific ocean first slightly shallows and then deepens by approximately 0.6 km (over the first 70 ky). Shoaling of the CCD produces two effects, which both contribute to the overall increase of $[Ca^{2+}]$. First, as the CCD shoals, a bigger fraction of the ocean floor is being exposed to undersaturated water, which directly lessens the amount of Ca^{2+} burial. Because weathering continues, this introduces a source/sink imbalance. The second effect is also linked to the CCD. As the CCD shallows and the saturation state of seawater with respect to carbonate minerals starts to decline, dissolving carbonates previously deposited to the sediments adds more Ca^{2+} to the seawater. This process is also known as seafloor neutralization [*Archer et al.*, 1997, 1998; *Ridgwell and Hargreaves*, 2007]. The overall $\Delta[Ca^{2+}]$ for the given scenario is illustrated in Figure 2g. After about 60 ky when the carbon input ceases, the calcium concentration still remains high (because of weak weathering feedback) and begins to return to the initial state after around 100 ky, facilitated by prolonged enhanced carbonate and silicate weathering.

5.1. Difference Between Carbonate and Silicate Weathering

[20] The results presented in Figures 3 and 4 serve to compare the separate impacts of increased carbonate weathering (no change in F_{Si}) and increased silicate weathering (no

Figure 5. Simulated change in $[Ca^{2+}]$ as a function of carbon input and simultaneous increase of both carbonate and silicate weathering fluxes.

change in F_C) on the $\Delta[Ca^{2+}]$, respectively. The simulation shows that at constant carbon input with increasing carbonate weathering, the $\Delta[Ca^{2+}]$ increases. On the contrary, the $\Delta[Ca^{2+}]$ decreases with increased F_{Si} at constant carbon input. There are two processes that are responsible for the observed incongruity. The first process is associated with the different magnitudes of the weathering fluxes F_C^0 (15.8×10^{12} mol C yr^{-1}) and F_{Si}^0 (5.7×10^{12} mol C yr^{-1}). The initial F_C^0 is already more than twice F_{Si}^0, thus the rate of delivery of calcium ions is larger with increased carbonate weathering as opposed to increased silicate weathering, producing a positive $\Delta[Ca^{2+}]$. The second and more important process that results in a different trend of $\Delta[Ca^{2+}]$ as a function of carbonate and silicate weathering is due to different influences of the silicate and carbonate weathering on total carbon in the ocean. One mole of carbonate delivered from the land to the ocean-atmosphere system adds one mole of calcium (on a net basis), one mole of TC and two moles of TA (equation (1) and Table 1). On the other hand, on this timescale silicate weathering does not affect the TC but has the same effect as carbonate weathering on TA and calcium (equation (2) and Table 1). The reason why TC is not affected by silicate weathering is that the atmosphere and ocean act as a single reservoir on timescales of several thousands of years. Thus,

the net change of TC is zero, since every two moles of carbon absorbed on continents from the ocean-atmosphere reservoir in form of the CO_2 return back to the ocean in the form of two moles of HCO_3^- (note that in steady state, burial of carbonate is balanced by volcanic input; Figure 6). However, ultimately silicate weathering of course sequesters carbon. The sequestration begins at the point when the net burial exceeds the net input of calcium ion and carbon is being sequestered in the form of $CaCO_3$. One could also argue that CO_2 sequestration starts when net burial exceeds the baseline riverine flux. In our model these two events occur approximately at the same time, around 100 ky in the standard run.
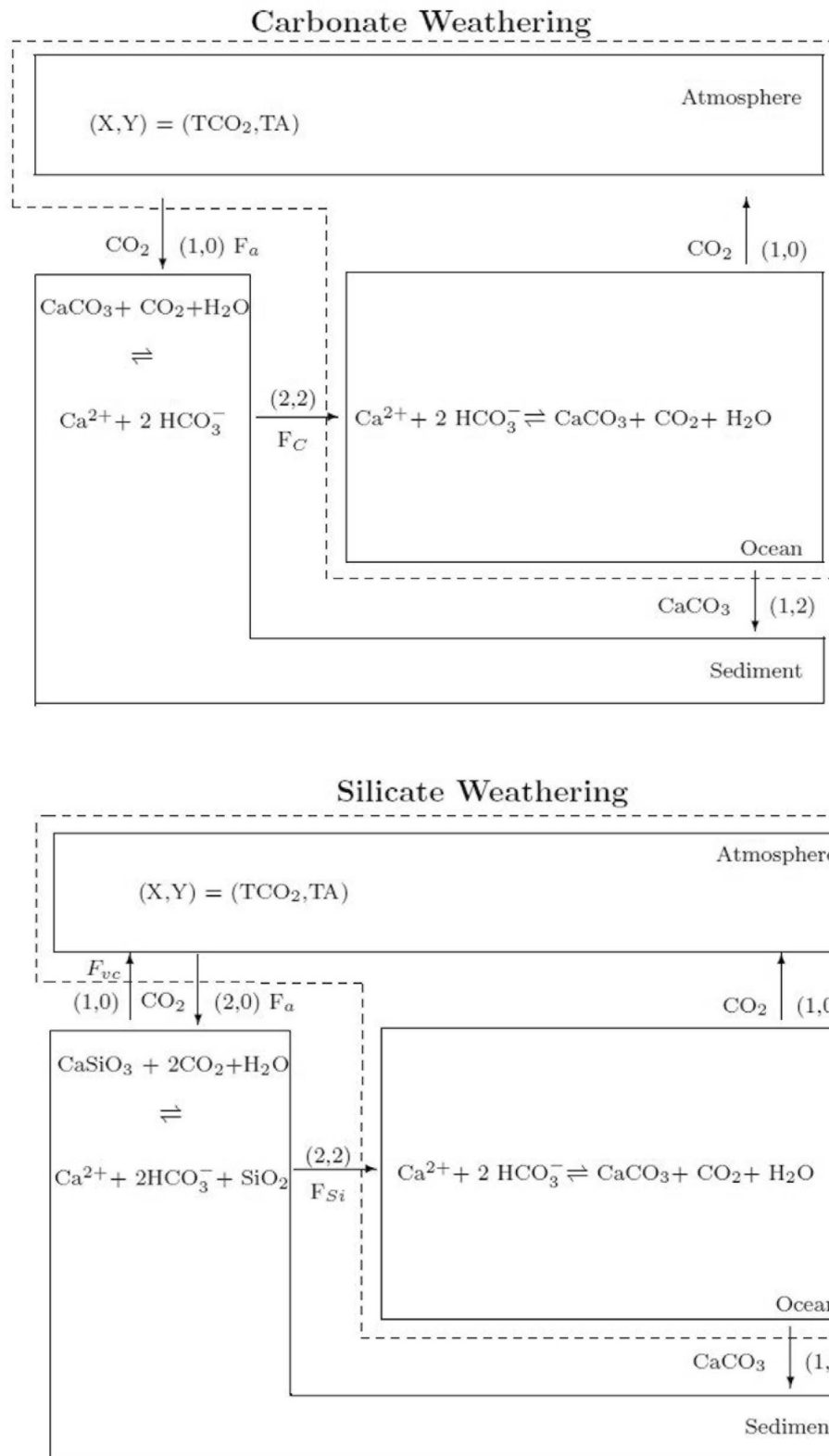
[21] With increased silicate weathering, the TC/TA ratio changes, increasing the alkalinity of seawater. This means

Table 1. Net Change (Mole) in Flux per One Mole of Weathered Ca^{2+} for Combined Ocean-Atmosphere System[a]

	Carbonate	Silicate
Ca^{2+}	+1	+1
TC	+1	0
TA	+2	+2

[a]See Figure 6 and equations (1) and (2). Only $F_C - F_a$ and $F_{Si} - F_a$, respectively, are considered. TC is total carbon, and TA is total alkalinity.

Carbonate Weathering

Silicate Weathering

Figure 6. Carbonate and silicate weathering fluxes. Compare with Table 2. X is total inorganic carbon, and Y is total alkalinity. On long timescales, the atmospheric and oceanic box act as a single reservoir, which is indicated by the dashed lines.

Table 2. The Effect of F_C and F_{Si} on the CCD and $\Delta[Ca^{2+}]^a$

Experiment	F_C^0 (mol C yr^{-1})	F_C	F_{Si}^0 (mol C yr^{-1})	F_{Si}	$\Delta[Ca^{2+}]$(%)	ΔCCD (km)
1	15.8	21.5	5.7	5.7	0.10	0.46
2	15.8	15.8	5.7	11.4	0.04	0.75

[a]After increasing both weathering rates independently by 5.7×10^{12} mol C yr^{-1} (Experiment 1: F_C increased; Experiment 2: F_{Si} increased), the effect of carbonate weathering increase on the CCD change is much less than that of silicate weathering.

that silicate weathering has a larger per-mole effect on the deepening of the CCD than carbonate weathering. This effect is illustrated in Table 2. As mentioned above, silicate and carbonate weathering were most likely simultaneously enhanced during the PETM (scenario 3). The effect of such an increase on $\Delta[Ca^{2+}]$ is shown in Figure 5 and essentially represents the sum of the scenarios shown in Figures 3 and 4. Among the three conditions, this is the one in which $\Delta[Ca^{2+}]$ is the least dependent on the amount of increased weathering.

5.2. Effect of Ca Inventory Changes on B/Ca and Mg/Ca

[22] Deep ocean carbonate saturation and temperature of past climate events have been reconstructed using the ratios of boron to calcium and magnesium to calcium, respectively [*Yu and Elderfield*, 2007; *Elderfield and Ganssen*, 2000]. One assumption used in those methods is that the concentration of Ca^{2+} does not fluctuate on timescales shorter than the residence time of calcium. Here we investigate whether the magnitude of carbon perturbation that occurred during the PETM was capable of changing the Ca^{2+} concentration enough to question the reliability of the above mentioned methods.

[23] The summary of our simulations is illustrated in Figure 5. The results represented here are derived from a variety of different scenarios in which the magnitude of silicate and carbonate weathering fluxes were simultaneously increased. The scale of carbon input ranged from 1,000 to 6,000 Pg C. This approach allows us to include plausible Ca changes ($\Delta[Ca^{2+}]$) during the PETM, thus giving us a range of scenarios. The $\Delta[Ca^{2+}]$ is greatest under the scenario where the input of carbon is 6,000 Pg C, regardless of the weathering sensitivity used (Figure 5). Under this scenario, Ca^{2+} increases by approximately 1.5%. Furthermore, according to *Zeebe et al.* [2009], the initial PETM carbon input was probably 3,000 Pg C or less. Also, *Zeebe et al.* [2009] calculated an increase in atmospheric CO_2 from a baseline of 1,000 ppmv to approximately 1,700 ppmv during the onset of the PETM. The increase in CO_2 can be compared to the results of the study by *Uchikawa and Zeebe* [2008], which covered the possible range of weathering fluxes as a function of pCO_2 as given by *Berner and Kothavala* [2001] and *Walker and Kasting* [1992]. Applying these findings to the estimated increase of pCO_2 during the main stage of the PETM (from 1,000 ppmv to 1,700 ppmv) suggests that the silicate weathering flux did not increase by more than 50% regardless of the model employed. The increase in carbonate weathering caused by the 700 ppm rise in pCO_2 is not more than 100% in any scenario presented by *Uchikawa and Zeebe* [2008]. By using the above mentioned results (carbon input ≤3,000 Pg C and weathering increase <100%) and comparing it to the results of our study, $\Delta[Ca^{2+}]$ during the main stage of

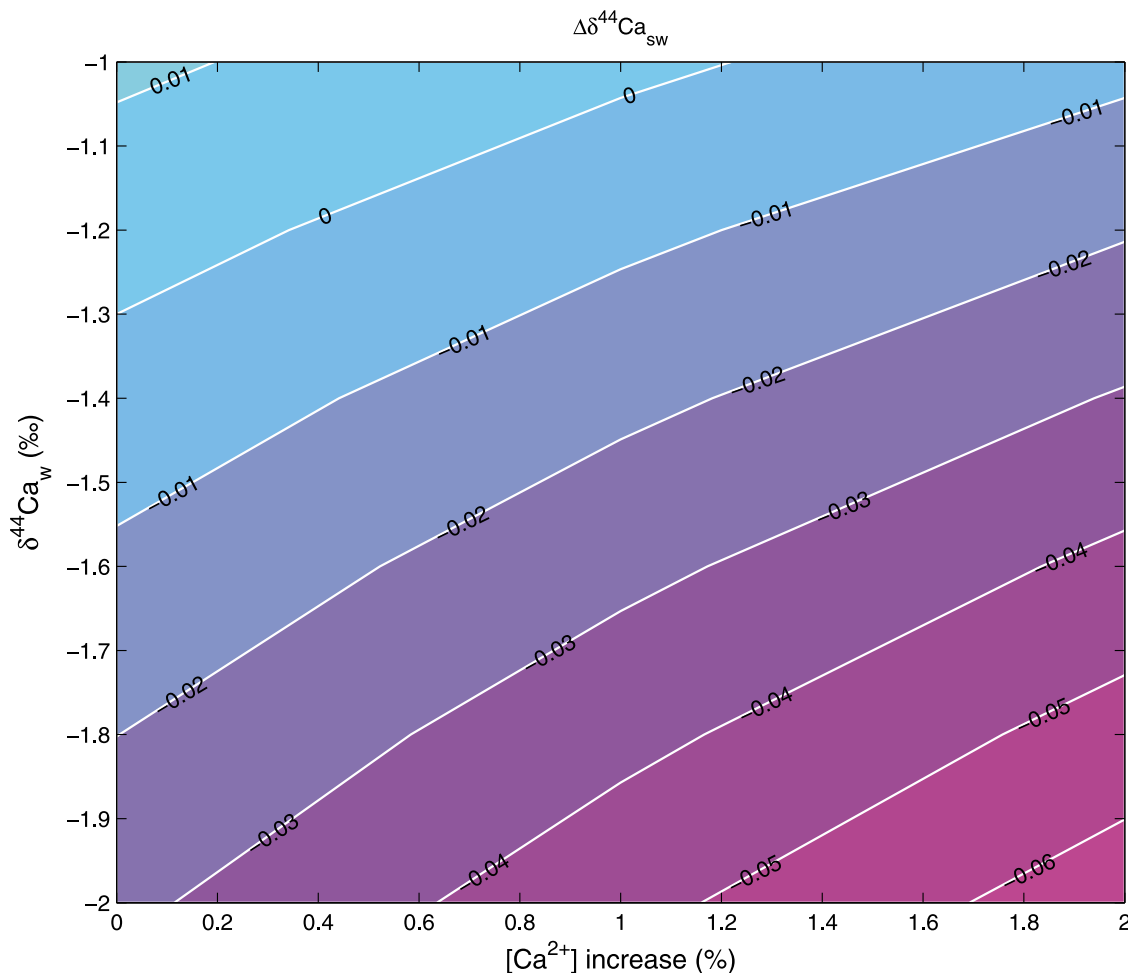the PETM was probably in the range of 0.07% to 0.7% (Figure 5, area below 3,000 Pg C).

[24] Even if the most extreme scenarios is assumed, when $\Delta[Ca^{2+}]$ is around 2% (Figure 3, top right corner) and when this change is applied to the equation for Mg/Ca ratio to temperature conversion of *Anand et al.* [2003], the calculated temperature uncertainty is approximately 0.2°C, which is within the uncertainty of ±1.2 to ±1.4°C given by *Anand et al.* [2003] and *Dekens et al.* [2002]. If the same change in calcium is applied to the equation for calculating the $\Delta[CO_3^{2-}]$ from B/Ca ratios of *Yu and Elderfield* [2007] the uncertainty is ~4 μmol kg^{-1} (*C. wuellerstorfi* species), which is within their uncertainty envelope of ±10 μmol kg^{-1}. This leads to the conclusion that the PETM carbon cycle perturbation was not large enough to disturb the calcium ion concentration to the extent that would question the feasibility of using B/Ca for reconstructing past variations in deep water carbonate saturation state or to question the reliability of the Mg/Ca method for reconstructing paleotemperatures. Nevertheless, there are other processes that could affect the reliability of the above mentioned methods (such as dissolution on the seafloor, diagenesis, vital effects, etc.), but they are beyond the scope of this study.

5.3. Effect on the Ocean Calcium Isotope Budget

[25] It has been speculated that throughout Earth's history, the isotopic composition of the marine calcium has varied considerably. This change is mainly driven by the imbalance between riverine and hydrothermal inputs of Ca^{2+} as well as the outputs via sedimentation of $CaCO_3$ on the seafloor [e.g., *De La Rocha and DePaolo*, 2000; *Schmitt et al.*, 2003; *Heuser et al.*, 2005]. As we showed here, such an inequality might have altered the seawater [Ca^{2+}] by up to 2% during the PETM (under the most extreme scenario) and consequently could cause an excursion of the seawater Ca isotope composition ($\delta^{44}Ca_{sw}$). Another factor responsible for changes in $\delta^{44}Ca_{sw}$ is the isotopic composition of the minerals that are being weathered ($\delta^{44}Ca_w$) as silicate and carbonate rocks have different $\delta^{44}Ca$ values. Accordingly, if the input of calcium from these weathering processes changed in the past, it would result in a different $\delta^{44}Ca_w$. In their study, *Griffith et al.* [2008] used values of $\delta^{44}Ca_w$ ranging from −1.8*l* to −1.2‰. Here we cover a wider range of possible $\delta^{44}Ca_w$ scenarios (−2.0‰ to −1.0‰). Our simulation is based on the following mass balance of the Ca isotopic composition of seawater:

$$N_{Ca} \frac{d(\delta^{44}Ca_{sw})}{dt} = F_{in}\left(\delta^{44}Ca_w - \delta^{44}Ca_{sw}\right) - F_{out}\left(\Delta^{44}Ca_{out}\right) \quad (8)$$

where N_{Ca} is the amount of Ca^{2+} in the ocean in moles, F_{in} is the flux of Ca^{2+} to the ocean from both silicate and carbonate weathering and hydrothermal inputs, F_{out} represents the flux of Ca^{2+} from the ocean due to carbonate sedimentation in mol yr^{-1} and $\Delta^{44}Ca_{out}$ is the difference between the Ca isotopic

Figure 7. Simulated change in $\delta^{44}Ca_{sw}$ as a function of $\delta^{44}Ca_w$ and increase in $[Ca^{2+}]$.

composition of marine carbonates and seawater in ‰. In steady state, F_{in} equals F_{out} and these values are initially set to 21.5×10^{12} mol yr^{-1} ($F_C^0 + F_{Si}^0$). In our study, we kept $\Delta^{44}Ca_{out}$ constant at -1.3‰ [*De La Rocha and DePaolo*, 2000; *Fantle and DePaolo*, 2005; *Griffith et al.*, 2008]. We solved equation (8) numerically for $\delta^{44}Ca_{sw}$, varying F_{in} in order to produce increases in N_{Ca} and thus the corresponding change in $[Ca^{2+}]$ (Figure 7). The largest change in $\delta^{44}Ca_{sw}$ ($\Delta\delta^{44}Ca_{sw}$) is produced when the $\Delta[Ca^{2+}]$ is 2% and when the Ca isotopic composition of the weathered material is -2‰. Under this scenario, the $\Delta\delta^{44}Ca_{sw}$ is around -0.06‰. As previously mentioned, because the $\Delta[Ca^{2+}]$ during the PETM was most likely less than 0.6%, it follows that the change in isotopic composition of seawater during the PETM was most likely less than -0.04‰. These results show that the Ca isotopic composition of seawater was essentially not affected by the carbon perturbation, it remained nearly constant over the PETM.

[26] Variations in the marine calcium cycle throughout the Earth's history have been reported but the factors responsible for the variations are only important over longer timescales (several hundreds of thousands to millions of years). Yet it is improbable that long-term processes affected the PETM (timescale ~200 ky). One hypothesis

suggests significant imbalances between input and output of Ca^{2+} from the ocean over the Cenozoic, which would be one possible explanation for variable calcium isotopic composition over this time period [*De La Rocha and DePaolo*, 2000; *Fantle*, 2010]. However, these processes, such as dolomite formation and decoupling of calcium riverine flux from the carbonate flux, affect seawater concentrations on multimillion year timescales.

6.   Conclusions

[27] In summary, our results show that dissolution and enhanced continental weathering had a small effect on the ocean's Ca^{2+} inventory during the PETM. Additional simulations showed that this conclusion also holds at modern seawater Ca^{2+} and Mg^{2+} concentrations. The small effect that is seen in this study differs among the carbonate and silicate weathering fluxes. Accelerated carbonate fluxes increase the $\Delta[Ca^{2+}]$ of the ocean. On the contrary, enhanced silicate fluxes show a tendency to decrease the $[Ca^{2+}]$ on the given timescale because increased silicate flux increases the alkalinity of seawater (TC/TA ratio changes), resulting in a larger per-mole effect on the deepening of the CCD than carbonate weathering. Since the effect of the silicate weathering over-

whelms the effect of the carbonate weathering, the overall result is that with the simultaneous increase of both fluxes, the $\Delta[Ca^{2+}]$ decreases or remains nearly constant. This is reflected in the almost horizontal lines in Figure 5. On the other hand, the $\Delta[Ca^{2+}]$ is highly dependent on the size of the carbon input. This implies that the effect of delivery of Ca^{2+} from the dissolution on the seafloor is much greater on the ocean Ca inventory than the effect that results from the continental runoff. By using the results from this study and combining them with the findings from two other studies [*Uchikawa and Zeebe*, 2008; *Zeebe et al.*, 2009], we were able to constrain the most plausible range of $\Delta[Ca^{2+}]$. The maximum increase of Ca^{2+} was most likely less than 0.7% relative to the concentration prior to the PETM; the maximum $\Delta[Ca^{2+}]$ is observed around 100 ky after the onset of the event when the carbon input ceases. Thus, the calculated temperature uncertainty (for the most extreme scenario, $\Delta[Ca^{2+}] = 2\%$) of 0.2°C and $\Delta[CO_3^{2-}]$ uncertainty of $\sim4 \ \mu mol \ kg^{-1}$ become even smaller; the $\Delta\delta^{44}Ca_{sw}$ is in the range from +0.01‰ to −0.04‰.

[28] We conclude that the magnitude of calcium ion change due to enhanced weathering and carbonate dissolution during the PETM is not large enough to affect the accuracy of proxies based on B/Ca and Mg/Ca ratios and $\delta^{44}Ca_{sw}$ via Ca^{2+} inventory changes. On multimillion time-scales, however, other processes control seawater calcium fluctuations such as dolomite formation [*Holland and Zimmermann*, 2000] and decoupling of calcium riverine flux from the carbonate flux [*Wallmann*, 2001; *Heuser et al.*, 2005].

Appendix A: Estimating the Effect of Dissolution on Seawater Calcium

[29] In order to estimate the volume of the sediment available for dissolution it is necessary to make a few assumptions. First, we assumed that the area of the entire ocean floor is equal to the area of the ocean surface (Aoc), which is $3.49 \times 10^{14} \ m^2$. If the CCD is at 3.5 km, then the area of the ocean floor above the CCD is approximately 30% of the entire ocean floor. A top sediment mixed layer of 10 cm was assumed (h_s). The density of sediments $\rho = 2.5 \ g \ cm^{-3}$. f_c is the carbonate fraction in dry sediments and a value of 0.71 was chosen (calculated by LOSCAR). The porosity of the sediments (ϕ) is 0.7. In order to calculate the mass of $CaCO_3$ in sediments above the CCD (M_{CaCO_3}) the following equation was employed:

$$M_{CaCO_3} = Aoc \times 0.3 \times h_s \times (1 - \phi) \times f_c \times \rho \quad (A1)$$

This gives an amount of 5.6×10^{18} g of $CaCO_3$ which is equal to 5.6×10^{16} moles of C ($\sim$670 Pg C) and as many moles of Ca^{2+} (m_{Ca}) since the molar ratio of carbon to calcium is 1:1. In order to get the percent change of $[Ca^{2+}]$ that such an input would produce, two more pieces of information are necessary: the mass of the ocean ($M_{oc} = 1.38 \times 10^{21}$ kg) and the seawater calcium concentration at the time of dissolution, which was taken as 20 mmol for the PETM ($[Ca]_{sw}$) [*Tyrrell and Zeebe*, 2004]:

$$\Delta[Ca^{2+}] = \frac{m_{Ca}}{M_{oc} \times [Ca]_{sw}} \times 100 = 0.20\% \quad (A2)$$

The calculated value of 0.20% for $\Delta[Ca^{2+}]$ is a lower estimate since it does not account for the variable porosity and the erosion of the sediments. Since the porosity and the erosion of the sediments in our model vary, the ratio of total $CaCO_3$ available during erosion to the mass contained in the original layer (M_{CaCO_3}) is given by:

$$1 + \frac{1 - \phi_0}{1 - \phi_1} \frac{f_c^0}{1 - f_c^0} \quad (A3)$$

where ϕ_0 and ϕ_1 are the porosities of a pure clay and calcite layer, respectively. The fraction $(1 - \phi_0)/(1 - \phi_1)$ is 0.4 in our calculation [*Zeebe and Zachos*, 2007]. Because f_c^0 was assumed to be 0.71, the fraction in the above equation is equal to 4. From equation (A3) it follows that the $CaCO_3$ available during erosion is approximately 2 times greater than the mass in the original surface layer (equation (A1)). Thus, the corrected $\Delta[Ca^{2+}]$ is actually 2 times larger and is approximately equal to 0.40% of the ocean's Ca inventory.

References

Anand, P., H. Elderfield, and M. H. Conte (2003), Calibration of Mg/Ca thermometry in planktonic foraminifera from a sediment trap time series, *Paleoceanography*, *18*(2), 1050, doi:10.1029/2002PA000846.

Archer, D., H. Kheshgi, and E. Maier-Reimer (1997), Multiple timescales for neutralization of fossil fuel CO_2, *Geophys. Res. Lett.*, *24*, 405–408.

Archer, D., H. Kheshgi, and E. Maier-Reimer (1998), Dynamics of fossil fuel CO_2 neutralization by marine $CaCO_3$, *Global Biogeochem. Cycles*, *12*, 259–276.

Berner, R. A., and Z. Kothavala (2001), GEOCARB III: A revised model of atmospheric CO_2 over Phanerozoic time, *Am. J. Sci.*, *304*, 397–437.

Berner, R. A., A. C. Lasaga, and R. M. Garrels (1983), The carbonate-silicate geochemical cycle and its effect on atmospheric carbon dioxide over the past 100 million years, *Am. J. Sci.*, *283*, 641–683.

Bice, K. L., and J. Marotzke (2002), Could changing ocean circulation have destabilized methane hydrate at the Paleocene/Eocene boundary?, *Paleoceanography*, *17*(2), 1018, doi:10.1029/2001PA000678.

Bowen, G. J., D. J. Beerling, P. L. Koch, J. C. Zachos, and T. Quattlebaum (2004), A humid climate state during the Paleocene-Eocene thermal maximum, *Nature*, *432*, 495–499.

Dekens, P. S., D. W. Lea, D. K. Pak, and H. J. Spero (2002), Core top calibration of Mg/Ca in tropical foraminifera: Refining paleotemperature estimation, *Geochem. Geophys. Geosyst.*, *3*(4), 1022, doi:10.1029/2001GC000200.

De La Rocha, C. L., and D. J. DePaolo (2000), Isotopic evidence for variations in the marine calcium cycle over the Cenozoic, *Science*, *289*, 1176–1178.

Dickens, G. R. (2000), Methane oxidation during the late Palaeocene thermal maximum, *Bull. Soc. Geol. Fr.*, *171*(1), 37–49.

Dickens, G. R. (2001), Carbon addition and removal during the Late Palaeocene thermal maximum: Basic theory with a preliminary treatment of the isotope record at ODP Site 1051, Blake Nose, in *Western North Atlantic Palaeogene and Cretaceous Palaeoceanography*, edited by D. Kroon, R. D. Norris, and A. Klaus, Geol. Soc. Spec. Publ., 183, 293–305.

Dickens, G. R., J. R. O'Neil, D. K. Rea, and R. M. Owen (1995), Dissociation of oceanic methane hydrate as a cause of the carbon isotope excursion at the end of the Paleocene, *Paleoceanography*, *10*, 965–971.

Dunkley Jones, T., A. Ridgwell, D. J. Lunt, M. A. Maslin, D. N. Schmidt, and P. J. Valdes (2010), A Paleogene perspective on climate sensitivity and methane hydrate instability, *Philos. Trans. R. Soc. A*, *368*, 2395–2415, 2010.

Elderfield, H., and G. Ganssen (2000), Past temperature and $\delta^{18}O$ of surface ocean waters inferred from foraminiferal Mg/Ca ratios, *Nature*, *405*, 442–445.

Fantle, M. S. (2010), Evaluating the Ca isotope proxy, *Am. J. Sci.*, *310*, 194–230.

Fantle, M. S., and D. J. DePaolo (2005), Variations in the marine Ca cycle over the past 20 million years, *Earth Planet. Sci. Lett.*, 237, 102–117.

Griffith, E. M., A. Paytan, K. Caldeira, T. D. Bullen, and E. Thomas (2008), A dynamic marine calcium cycle during the past 28 million years, *Science*, 322, 1671–1674.

Heuser, A., A. Eisenhauer, F. Böhm, K. Wallmann, N. Gussone, P. N. Pearson, T. F. Nägler, and W.-C. Dullo (2005), Calcium isotope ($\delta^{44/40}$Ca) variations of Neogene planktonic foraminifera, *Paleoceanography*, 20, PA2013, doi:10.1029/2004PA001048.

Holland, H. D., and H. Zimmermann (2000), The dolomite problem revisited, *Int. Geol. Rev.*, 42, 481–490.

Horita, J., H. Zimmermann, and H. D. Holland (2002), Chemical evolution of seawater during the Phanerozoic: Implications from the record of marine evaporites, *Geochim. Cosmochim. Acta*, 66(21), 3733–3756.

Kelly, D. C., J. C. Zachos, T. J. Bralower, and S. A. Schellenberg (2005), Enhanced terrestrial weathering/runoff and surface ocean carbonate production during the recovery stages of the Paleocene-Eocene thermal maximum, *Paleoceanography*, 20, PA4023, doi:10.1029/2005PA001163.

Kennett, J. P., and L. D. Stott (1991), Abrupt deep-sea warming, palaeoceanographic changes and benthic extinctions at the end of the Palaeocene, *Nature*, 353, 225–229.

Kiessling, W., E. Flügel, and J. Golonka (2003), Patterns of phanerozoic carbonate platform sedimentation, *Lethaia*, 36(3), 195–225.

Koch, P. L., J. C. Zachos, and P. D. Gingerich (1992), Correlation betwen isotope records in marine and continental carbon reservoirs near the Paleocene/Eocene boundary, *Nature*, 358, 319–322.

Lea, D. W., D. K. Pak, and H. J. Spero (2000), Climate impact of late Quaternary equatorial Pacific sea surface temperature variations, *Science*, 289, 1719–1724.

Lowenstein, T. K., M. N. Timofeeff, S. T. Brennan, L. A. Hardie, and R. V. Demicco (2001), Oscillation in Phanerozoic seawater chemistry: Evidence from fluid inclusions, *Science*, 294, 1086–1088.

Morse, J. W., and F. T. Mackenzie (1990), *Geochemistry of Sedimentary Carbonates*, *Dev. Sedimentol.*, vol. 48, Elsevier, Amsterdam.

Pagani, M., K. Calderia, D. Archer, and J. C. Zachos (2006), An ancient carbon mystery, *Science*, 314, 1556–1557.

Panchuk, K., A. Ridgwell, and L. R. Kump (2008), Sedimentary response to Paleocene-Eocene thermal maximum carbon release: A model-data comparison, *Geology*, 36(4), 315–318, doi:10.1130/G24474A.1.

Ravizza, G., R. N. Norris, J. Blusztajn, and M.-P. Aubry (2001), An osmium isotope excursion associated with the late Paleocene thermal maximum: Evidence of intensified chemical weathering, *Paleoceanography*, 16, 155–163.

Ridgwell, A., and J. C. Hargreaves (2007), Regulation of atmospheric CO_2 by deep-sea sediments in an Earth system model, *Global Biogeochem. Cycles*, 21, GB2008, doi:10.1029/2006GB002764.

Ridgwell, A., and D. N. Schmidt (2010), Past constraints on the vulnerability of marine calcifiers to massive carbon dioxide release, *Nat. Geosci.*, 3, 196–200.

Ridgwell, A., and R. E. Zeebe (2005), The role of the global carbonate cycle in the regulation and evolution of the Earth System, *Earth Planet. Sci. Lett.*, 234, 299–315.

Robert, C., and J. P. Kennett (1994), Paleocene and Eocene kaolinite distribution in the South Atlantic and Southern Ocean: Antarctic climatic and paleoceanographic implications, *Mar. Geol.*, 103, 99–110.

Rosenthal, Y., E. A. Boyle, and N. Slowey (1997), Environmental controls on the incorporation of Mg, Sr, F and Cd into benthic foraminifera shells from Little Bahama Bank: Prospects for thermocline paleoceanography, *Geochim. Cosmochim. Acta*, 61, 3663–3643.

Schmitt, A. D., F. Chabaux, and P. Stille (2003), The calcium riverine and hydrothermal isotopic fluxes and the oceanic calcium mass balance, *Earth Planet. Sci. Lett.*, 213, 503–518.

Schmitz, B., and V. Pujalte (2007), Abrupt increase in seasonal extreme precipitation at the Paleocene-Eocene boundary, *Geology*, 35, 215–218.

Sluijs, A., et al. (2006), Subtropical Arctic Ocean temperatures during the Palaeocene/Eocene thermal maximum, *Nature*, 441, 610–613.

Thomas, D. J., T. J. Bralower, and C. E. Jones (2003), Neodymium isotopic reconstruction of late Paleocene-early Eocene thermohaline circulation, *Earth Planet. Sci. Lett.*, 209, 309–322.

Thomas, E. (2007), Cenozoic mass extinctions in the deep sea; what disturbs the largest habitat on Earth?, in *Large Ecosystem Perturbations: Causes and Consequences*, edited by S. Monechi, R. Coccioni, and M. Rampino, *Spec. Pap. Geol. Soc. Am.*, 424, 1–24.

Tyrrell, T., and R. E. Zeebe (2004), History of carbonate ion concentration over the last 100 million years, *Geochim. Cosmochim. Acta*, 68(17), 3521–3530.

Uchikawa, J., and R. E. Zeebe (2008), Influence of terrestial weathering on ocean acidification and the next glacial inception, *Geophys. Res. Lett.*, 35, L23608, doi:10.1029/2008GL035963.

Walker, J. C. G., and J. F. Kasting (1992), Effects of fuel and forest conservation on future levels of atmospheric carbon dioxide, *Palaeogeogr. Palaeoclimatol. Palaeoecol.*, 97, 151–189.

Walker, J. C. G., P. B. Hays, and J. F. Kasting (1981), Negative feedback mechanism for the long-term stabilization of Earth's surface temperature, *J. Geophys. Res.*, 86, 9776–9782.

Wallmann, K. (2001), Controls of hte Cretaceous and Cenozoic evolution of seawater composition, atmospheric CO_2 and climate, *Geochim. Cosmochim. Acta*, 65, 3005–3025.

Webb, A., L. R. Leighton, S. A. Schellenberg, E. A. Landau, and E. Thomas (2009), Impact of the Paleocene-Eocene thermal maximum on deep-ocean microbenthic community structure: Using rank-abundance curves to quantify paleoecological response, *Geology*, 37, 783–786.

White, A. F., and A. F. Blum (1995), Effects of climate on chemical weathering in watersheds, *Geochim. Cosmochim. Acta*, 59, 1729–1747.

Yu, J., and H. Elderfield (2007), Benthic foraminiferal B/Ca ratios reflect deep water carbonate saturation state, *Earth Planet. Sci. Lett.*, 258, 73–86.

Yu, J., H. Elderfield, and B. Hönisch (2007), B/Ca in planktonic foraminifera as a proxy for surface seawater pH, *Paleoceanography*, 22, PA2202, doi:10.1029/2006PA001347.

Zachos, J. C., M. Pagani, L. Sloan, E. Thomas, and K. Billups (2001), Trends, rhythms, and aberrations in global climate 65 Ma to present, *Science*, 292, 686–693.

Zachos, J. C., M. W. Wara, S. Bohaty, M. L. Delaney, M. R. Petrizzo, A. Brill, T. J. Bralower, and I. Premoli-Silva (2003), A transient rise in tropical sea surface temperature during the Paleocene-Eocene thermal maximum, *Science*, 302, 1551–1554.

Zachos, J. C., et al. (2005), Rapid acidification of the ocean during the Paleocene-Eocene thermal maximum, *Science*, 308, 1611–1615.

Zachos, J. C., G. R. Dickens, and R. E. Zeebe (2008), An early Cenozoic perspective on greenhouse warming and carbon-cycle dynamics, *Nature*, 451, 279–283, doi:10.1038/nature06588.

Zeebe, R. E., and P. Westbroek (2003), A simple model for the $CaCO_3$ saturation state of the ocean: The "Strangelove," the "Neritan," and the "Cretan" Ocean, *Geochem. Geophys. Geosyst.*, 4(12), 1104, doi:10.1029/2003GC000538.

Zeebe, R. E., and D. A. Wolf-Gladrow (2001), *CO_2 in Seawater: Equilibrium, Kinetics, Isotopes*, Elsevier Oceanogr. Ser., vol. 65, 346 pp., Elsevier, Amsterdam.

Zeebe, R. E., and J. C. Zachos (2007), Reversed deep-sea carbonate ion basin gradient during Paleocene-Eocene thermal maximum, *Paleoceanography*, 22, PA3201, doi:10.1029/2006PA001395.

Zeebe, R. E., J. C. Zachos, K. Caldeira, and T. Tyrrell (2008), Oceans: Carbon emissions and acidification, *Science*, 321, 51–52, doi:10.1126/science. 1159124.

Zeebe, R. E., J. C. Zachos, and G. R. Dickens (2009), Carbon dioxide forcing alone insufficient to explain Paleocene-Eocene thermal maximum warming, *Nat. Geosci.*, 2, 576–580, doi:10.1038/NGEO578.

N. Komar and R. E. Zeebe, Department of Oceanography, School of Ocean and Earth Science and Technology, University of Hawaii at Manoa, 1000 Pope Rd., MSB 507, Honolulu, HI 96822, USA. (komar@hawaii.edu)